sciendo

Polish Journal of Chemical Technology, 20, 4, 66—74, 10.2478/pjct-2018-0056

Preparation, Characterization, and Application of N,S-codoped TiO_2/Montmorillonite Nanocomposite for the Photocatalytic Degradation of Ciprofloxacin: Optimization by Response Surface Methodology

Mohamadreza Massoudinejad[1], Ali Paseban[1*], Ahmadreza Yazdanbakhsh[1], Mohammad Reza Nabid[2]

[1]*Shahid Beheshti University of Medical Sciences, Department of Environmental Health Engineering, School of Health, P.CODE: P.C. 1983535511, Tehran, Iran.*
[2]*Shahid Beheshti University, Department of Chemistry, G.C., 1983963113, Tehran, Iran.*
[*]*Corresponding authors e-mail: ali.paseban@sbmu.ac.ir*

An N,S-codoped TiO_2/Montmorillonite nanocomposite, as a photocatalyst, was synthesized in the sol-gel method and used for the degradation of ciprofloxacin (Cip) in an aqueous solution. N,S-codoped TiO_2/Montmorillonte was characterized by powder X-ray diffraction (XRD), UV-Vis diffuse reflectance spectroscopy (DRS), field emission scanning electron microscopy (FESEM), transmission electron microscope (TEM), and X-ray fluorescence (XRF) analyzes. A central composite design (CCD) was used to optimize the variables for the removal of Cip by the N,S-codoped TiO_2/Montmorillonite. A maximum decomposition of 92% of Cip was achieved in optimum conditions. The band gap value for the nanocomposite was 2.77 eV. Moreover, with the use of nanocomposite in the four consecutive runs, the final removal efficiency was 66%. The results show that the N,S-codoped TiO_2/Montmorillonite under simulated sunlight irradiation can be applied as an effective photocatalyst for the removal of Cip from aqueous solutions.

Keywords: N,S-codoped TiO_2/Montmorillonite, nanocomposite, Ciprofloxacin, simulated sunlight, photocatalyst.

INTRODUCTION

Antibiotics have been recognized as an emerging environmental problem over the past few years[1]. Ciprofloxacin (Cip) -an effective factor against various bacteria- is widely used in human and veterinary medicine[2]. Cip is a low biodegradable pollutant that has toxic effects on human health; moreover, it can spread resistant bacteria that have negative effects on aquatic organisms[2, 3]. Because of persistent and non-biodegradability of Cip conventional treatment processes are not effective methods for its removal[4]. Therefore, most antibiotics, including Cip, will eventually reach aquatic ecosystems. Based on the results of some studies, Cip has been detected in a range of concentrations 3–87 μg L^{-1} in hospitals effluents and almost 31 mg L^{-1} in pharmacies factory effluents[5–7] 30, and 40°C. Therefore, the removal of this pollutant from aquatic environments is mandatory[8]. Heterogeneous photocatalytic degradation is one of the advanced oxidation processes that provide good technology for the removal of persistent organic pollutants[9]. Titanium dioxide (TiO_2) powder one of the most important photocatalysts is widely used in the treatment of organic pollutants, due to its properties such as high oxidation efficiency, non-toxicity, cost-effectiveness and structural stability[10–12] with the objective to tune shift their optical absorption from the UV towards the visible. The N-doped TiO_2 consist of nanostructured anatase phase with average TiO_2 nanocrystallite size of 29 nm. The nitrogen doping is clearly shown to produce the desired red shift of the absorption onset of the TiO_2 coatings (from ~380 nm to ~550 nm. But, due to the large bandgap of TiO_2, only a small UV portion of solar light (3–5%) can be used[13] visible light active, N, S-codoped TiO_2-based photocatalyst was prepared by reacting thiourea with nanoparticulate anatase TiO_2. Commercial anatase powders were manually ground with thiourea and annealed at 400 \u00b0C in two crucibles with different surface-to-volume ratios (S/V = 20 and 1.5. Also, application of TiO_2 powder in the heterogeneous photocatalytic degradation process involves limitations, including small specific surface area, low adsorption capacity, recovery problems, and agglomeration, which results in low photocatalytic efficiency[14, 15]. To maximize the efficiency of visible light, (42% of the energy of the solar spectrum), many efforts have been made to improve the photocatalytic properties of TiO_2 and its response to visible light[15]. An effective method to resolve these problems and extend the spectral response of TiO_2 to visible light is the doping of TiO_2 by adding non-metals (N, S, C, F)[13] visible light active, N, S-codoped TiO_2-based photocatalyst was prepared by reacting thiourea with nanoparticulate anatase TiO_2. Commercial anatase powders were manually ground with thiourea and annealed at 400 \u00b0C in two crucibles with different surface-to-volume ratios (S/V = 20 and 1.5. TiO_2 co-doped with two kinds nan-metal atoms simultaneously has attracted attention because of the synergistic effect permitting to tune the electronic structure and to intensify the visible-light photocatalytic activity[16, 17]. Although non-metal doping reduces the TiO_2 bond gap and improves the use of visible light, it cannot increase the specific surface and catalytic adsorption capability of TiO_2[15]. In order to overcome the limits of TiO_2, in some studies, supports such as montmorillonite (MMT) have been used[18, 19]. MMT shows a high adsorption capacity for Cip antibiotic due to its large special surface, ion exchange capacity, and layered structure[20]. In some studies, with the immobilization of TiO_2 on the MMT, functional composites have been synthesized[19, 21, 22]. The synthesized composite based on MMT, due to its high surface area and adsorption properties, can improve

the contact between the catalyst and organic contaminants, thus exacerbating organic matter photocatalytic degradation[21, 23].

It has been reported that TiO_2/MMT nanocomposite has been exhibited high photocatalytic activity under ultraviolet (UV) irradiation for degradation of Cip from polluted water[4, 24]. But mentioned nanocomposite exhibited little photocatalytic activity under the sunlight. Because, wide band gap of TiO_2 limits its photoresponse in the UV region, which is only a small fraction (3–5%) of the solar spectrum corresponding[25]. Therefore, it can be deduced that by non-metal dopping of TiO_2 and then immobilizing it onto the porous MMT with high adsorption properties, a narrow band gap nanocomposite as N,S-codoped TiO_2/MMT can be obtained, which, in addition to having high photocatalytic activity under the visible light, has better surface properties. Therefore, the main objective of this study is the synthesis and characterization of N,S-codoped TiO_2/MMT, and its application for heterogeneous photocatalytic degradation of Cip in aqueous solution under visible light.

MATERIAL AND METHODS

MATERIAL

MMT (K10) and titanium tetrachloride ($TiCl_4$, purum, ≥ 98.0%) and TiO_2 nanoparticle (99.7%) were purchased from (Sigma-Aldrich, USA). Thiourea (99%), acetonitrile (99.9%), and methanol (99.9%) were purchased from Merck Co. (Germany). Analytical grade Cip (≥ 98%) was purchased from Daroopakhsh Pharmaceutical Co. (Iran). All other chemicals, with the analytical grade, were purchased from Merck Co. (Germany).

PREPARATION OF N,S-CODOPED TIO_2/MMT

N,S-codoped TiO_2/MMT nanocomposite was prepared by the sol-gel process[26]. MMT, $TiCl_4$, and thiourea were used as the precursors of N,S-codoped TiO_2/MMT nanocomposite. For the synthesis of N,S-codoped TiO_2/MMT, 2.63 mL of $TiCl_4$ was slowly added to 10 mL of 6 mol L^{-1} hydrochloric acid solution, followed by successive stirring and dilution with deionized water. Then, 38.37 mL of thiourea solution (2.5 mol L^{-1}) was added dropwise to the prepared solution while stirring. This solution was then added dropwise into 100 mL suspension of MMT in deionized water under vigorous stirring. The resulting product was picked out and washed with deionized water several times, and then dried in a vacuum oven at 80°C and calcined at 350°C in air for two hours.

CHARACTERIZATION METHODS

The crystalline phase of the nanomaterials was characterized using the XRD (X' Pert Pro, Netherlands) technique. Field emission scanning electron microscopy (FESEM) (SIGMA VP-500, Zeiss, Germany), and transmission electron microscope (TEM), (EM10C, Zeiss) was employed to detect the particle size and morphology of the nanomaterials. The textural properties of the samples were obtained based on nitrogen adsorption-desorption (BElSORP Mini, Microtrac Bel Corp, Japan) at 77 K and calculated according to isotherm models of Brunauer-Emmett-Teller, (BET) and Barett-Joyner-Halenda (BJH). The chemical composition of the samples was determined by an X-ray fluorescence (XRF) spectrometer (ED 2000, Oxford Instrument, UK). Uv-vis diffuse reflectance spectroscopy (DRS) (UV-2550, Shimadzu, Japan) samples were determined.

PHOTOCATALYTIC EXPERIMENTS

The heterogeneous photocatalytic reaction was carried out in a cylindrical batch reactor with a working volume of 1000 m L^{-1} (Fig. 1). Two Xenon lamps (2×55 W, Philips, Netherlands) were used as the simulated sunlight source. The xenon lamps were positioned inside a quartz tube in the photoreactor to ensure the highest light availability in the photoreactor. The intensity of simulated sunlight, measured with a Lux meter, was 30000 Lux with a wavelength range of 380–900 nm. In order to remove the heat from the xenon lamps, a fan was placed under the reactor. The temperature of the reaction solution was kept constant at 28 ±1°C using a water-filled jacket connected to a recirculation cooler. An air pump equipped with a circular bubble diffuser at the bottom of the photoreactor was utilized for suspending photocatalyst particles to achieve an average equal exposure.

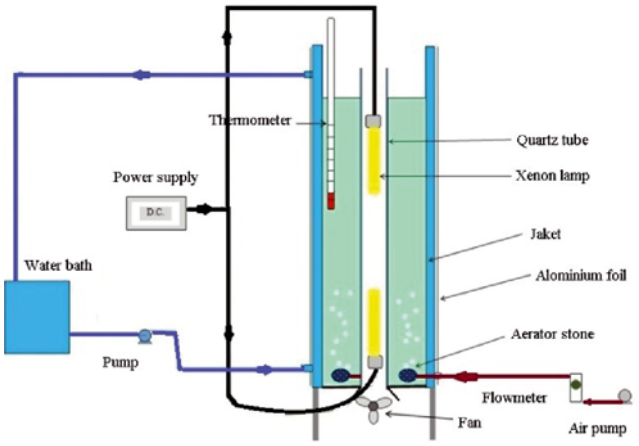

Figure 1. Schematic image of the photoreactor used for Cip photodegradation

ANALYTICAL METHODS

The concentration of Cip during the experiments was analyzed using a high performance liquid chromatography (HPLC) instrument (Knauer, Germany) equipped with a reversed phase column (C18 ODS 5 μm, 250 × 4.6 mm) with a UV detector at a wavelength of 276 nm. The mobile phase consisted of 0.017 mol L^{-1} phosphoric acid and acetonitrile at a ratio of 80: 20. Oven temperature was kept at 30°C during analysis. The flow rate was 1 mL min^{-1} and the sample volume was 20 µ L.

EXPERIMENTAL DESIGN AND VARIABLES

In the present study, central composite design (CCD), one of the forms of response surface methodology (RSM), was used for the optimization of photocatalytic degradation process. The CCD contain five levels (–α, –1, 0, +1, and +α) with four independent variables include Cip concentration (5, 10, 15, 20 and 25 mg L^{-1}), catalyst dose (12.5, 25, 37.5, 50 and 62.5 mg L^{-1}), pH (3, 5, 7, 9 and 11) and reaction time (15, 40, 65, 90 and 115 min).

Eq. (1) was applied to explain the effect of independent variables in the second-order polynomial model:

$$Y(\%) = a_0 + \sum_{i=1}^{n} a_{ii} X_i^2 + \sum_{i-1}^{n-1} \sum_{j-2}^{n} a_{ij} X_i X_j + e \qquad (1)$$

where Y is the response (efficiency removal), a_0 is the intercept value, a_i, a_{ii}, and a_{ij} are regression coefficients, x_i and x_j are the independent variables, and e is the random error [9]. Analysis of variance was used to find the interaction between the independent variables and the response.

RESULTS AND DISCUSSION

XRD PATTERN OF NANOMATERIALS

The XRD patterns of MMT and N, S-codoped TiO_2/MMT are illustrated in Fig. 2a, b, respectively. As can be seen in Fig. 2a, the peaks at 2θ of 19.9°, 35.02°, 54.2°, and 61.87° are characteristic of MMT (JCPDS Card No. 002-0037). In the XRD pattern of N, S-codoped TiO_2/MMT, in addition to the peaks correspond to MMT, there are peaks that correspond to the anatase and rutile phases. The peaks at 2θ of 25.3°, 37.3°, and 48.2° are related to the anatase (JCDPS 21-1272), and the peaks at 2θ of 27.5°, 36.0°, 54.2°, and 69.3° are related to the rutile (JCDPS 21-1276) (Fig. 2b). The XRD results clearly showed that the N,S-codoped TiO_2/MMT nanocomposite consists of both anatase and rutile phases. There is high catalytic activity in the crystalline structures containing anatase and rutile[27] Box-Behnken design (BBD). The presence of TiO_2 peaks in the XRD pattern of nanocomposite shows that the TiO_2 nanoparticles have been stabilized on the surface of the MMT[3]. The results obtained from the analysis of the XRD pattern by applying the Debye-Scherrer equation reveals that the average size of N,S-codoped TiO_2/MMT was 24 nm. Experiment XRD results showed that N,S-codoped TiO_2 crystals have been well-loaded onto the MMT surface by the sol-gel method.

XRF ANALYSIS

The XRF analysis results indicate the chemical composition of MMT and N,S-codoped TiO_2/MMT nanocomposite (Table 1).

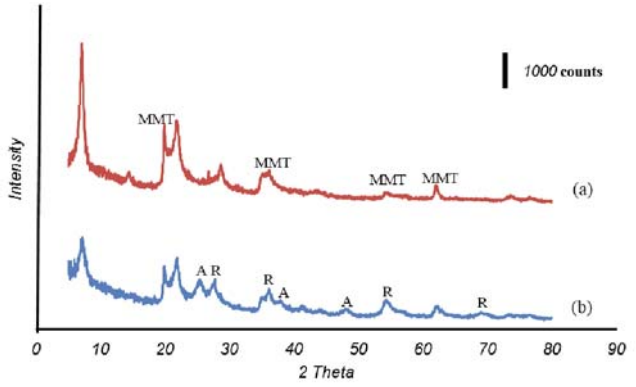

Figure 2. XRD pattern of (a) MMT and (b) N,S-codoped TiO_2/MMT nanocomposite (A = Anatase, R = Rutile, MMT = Montmorillonite)

The composition of MMT in terms of weighting percent is as follows: SiO_2: 84.5%, Al_2O_3: 9.1%, CaO: 2.1%, and other compounds. But the weight percent of these compounds in the N,S-codoped TiO_2/MMT nanocomposite is as follows: SiO_2: 50.4%, TiO_2: 39.3%, Al_2O_3: 6.2%, and others. The weight percent of TiO_2 in N,S-codoped TiO_2/MMT nanocomposite is significantly higher than MMT. Increasing the weighting percent of TiO_2 in synthesized N,S-codoped TiO_2/MMT nanocomposite indicates that TiO_2 nanoparticles were stabilized on the surface of MMT, which matches the results of XRD. These results have a strong agreement with result of Hassani[4].

Table 1. MMT and N,S-codoped TiO_2/MMT, chemical composition

Compound	MMT [wt. %]	N,S-codoped TiO_2/MMT [wt. %]
SiO_2	84.5	50.4
Al_2O_3	9.1	6.2
CaO	2.1	0.2
Fe_2O_3	1.4	0.6
MgO	1.1	1.0
P_2O_5	0.8	0.6
TiO_2	0.4	39.3
SO_3	–	0.6
Other	0.6	1.1

FE-SEM AND TEM OF NANOMATERIALS

FESEM images were utilized to study the morphology of the MMT and N,S-codoped TiO_2/MMT nanocomposite. Figure 3a, b show the FESEM of MMT and N,S-codoped TiO_2/MMT samples. MMT has a layered structure with a non-uniform size distribution and an uneven surface morphology[4]. FESEM of N,S-codoped TiO_2/MMT sample indicates that fine N,S-codoped TiO_2 particles were stabilized on the surface of MMT (Fig. 3b). These results are consistent with those of study[26]. Based on the results of the FESEM, it can be concluded that the sol-gel method is a reliable method for the synthesis of N,S-codoped TiO_2/MMT nanocomposites.

The TEM image was used to study morphology, particle size, and crystallinity of the nanomaterials (Fig. 3c, d). Figure 3c shows the porous surface of the MMT. As can be observed in Figure 3d, the deposited N,S-codoped TiO_2 nanoparticles accumulated on the surface of the MMT. The immobilized N,S-TiO_2 nanoparticles on of MMT surface have a mean value in the range of 20 to 30 nm, confirming the results of the FESEM analysis, and have an agreement with the XRD measurements using Debye–Sherrer's equation.

OPTICAL PROPERTIES OF NANOMATERIALS

The DRS of the MMT and N,S-codoped TiO_2/MMT samples are shown in Figure 4a. Figure 4 shows that the N,S-TiO_2-MMT has a stronger absorption edge and a shift to the visible light region as compared to that of undoped TiO_2. The transformed Kubelka–Munk function is used to estimate the band gap energy by plotting $[F(R\infty) * h\upsilon]^{0.5}$ Vs. $h\upsilon$ (Fig. 4b). Generally, nonmetal doping of TiO_2 can reduce band gap value. Results of this examination depict that band gap value of samples has decreased from 3.17 eV (un-doped TiO_2) to 2.77 eV (N,S-codoped TiO_2). Due to the reduction of the nanocomposite band gap, it can be easily used as

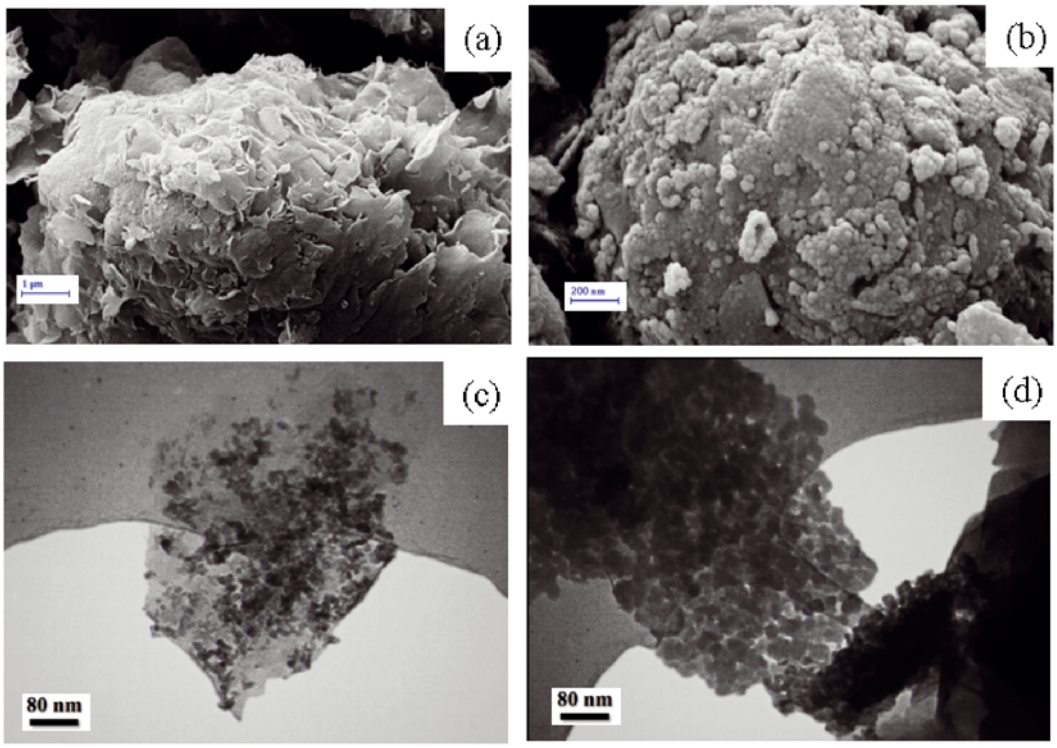

Figure 3. Images of (a) FESEM of MMT, (b) FESEM of N,S-codoped TiO_2/MMT, (c) TEM of MMT and (d) TEM of N,S-TiO_2--MMT

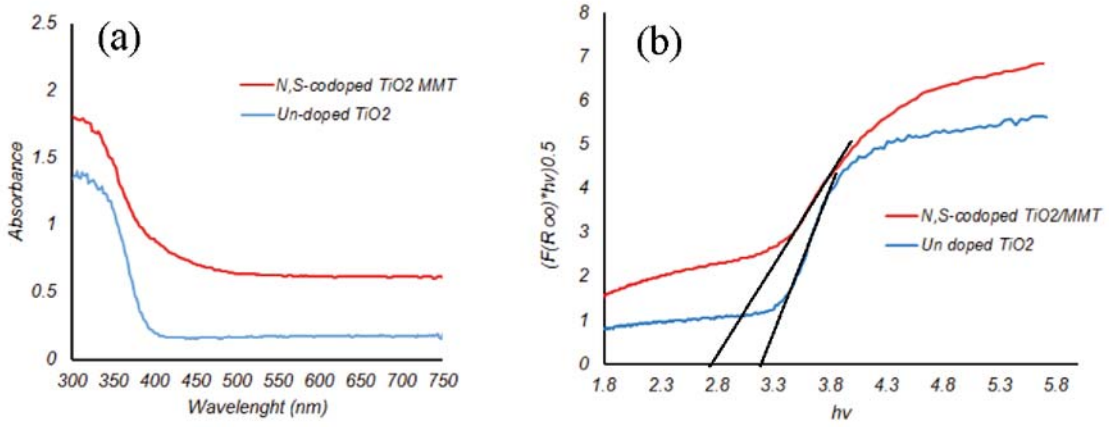

Figure 4. (a) UV-visible diffuse absorption spectra and (b) Plots of [F (R∞) * hυ]$^{0.5}$ vs. photon energy (hυ) of N,S-codoped TiO_2/MMT, and Undoped TiO_2

a photocatalyst under simulated sunlight. These results are consistent with the results of other researchers [15,16].

BET & BJH OF NANOMATERIALS

Nitrogen adsorption and desorption isotherms were used to determine the specific surface area and porosity of nanomaterials. As shown in Figure 5, the presence of a hysteresis loop at relative pressure of 0.4 to 1.0, indicating the presence of mesopores (type IV)[26, 28]. The specific surface area and pore volume of the N,S--codoped TiO_2/MMT nanocomposite are 131.4 $m^2\ g^{-1}$ and 0.3 $cm^3\ g^{-1}$, respectively (Table 2 and Fig. 5). The results showed that the N, S-codoped TiO_2/MMT has a higher surface area and porosity than those of MMT. These results have agreement with results of Fatimah[29]. The synthesis of doped TiO_2 with some elements by the sol-gel method can increase the special surface areas depending on the nature of the doping agent[30]. Increasing the specific surface area in N,S-codoped TiO_2/MMT nanocomposite indicates that N,S-codoped TiO_2 particles have been inserted into pores of the MMT, creating a three-dimensional pillard structure[31]. A high surface area and high porosity catalyst is useful for photocatalytic activity in terms of mass transfer and increases the catalyst's ability to transfer molecules[32].

Sample	Specific surface area [$m^2\ g^{-1}$]	Total pore volume [$cm^3\ g^{-1}$]	Average pore diameter [nm]
MMT	79.5	0.2	11
N,S-codoped TiO_2/MMT	131.4	0.3	9

Table 2. Textural characteristics of MMT and N,S-codoped TiO_2/MMT nanocomposite samples

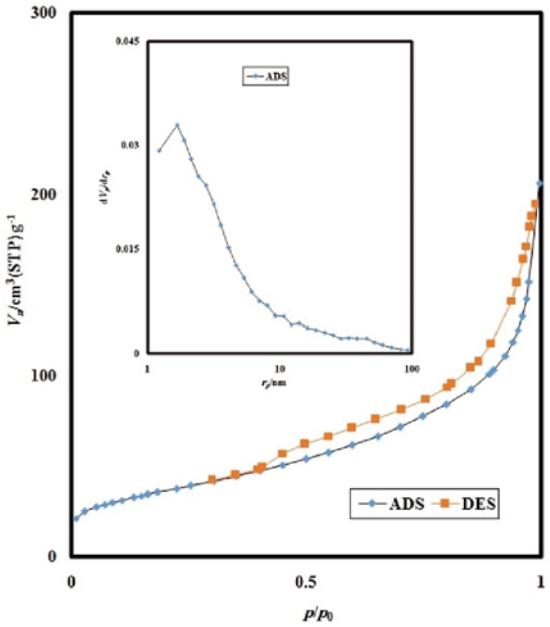

Figure 5. ADS, DES and BJH plot of N,S-TiO_2-MMT nanocomposite

PRELIMINARY STUDIES

Preliminary experiments were carried out to evaluate the effect of photolysis and adsorption on removal of Cip. Photolysis experiments were carried out at pH of 6, initial Cip 15 mg L^{-1}, irradiation time 115 min, and without catalyst. Adsorption experiments were carried out at pH of 6, initial Cip 15 mg L^{-1}, reaction time 115 min, and catalyst dose of 45 mg L^{-1} without visible light irradiation. The maximum removal values of Cip in 90 min by photolysis and adsorption were 26% and 33% respectively (Fig. 6).

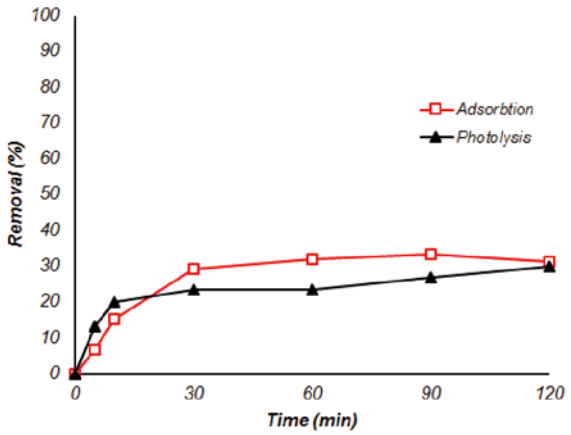

Figure 6. Effect of photolysis and adsorption of removal with the synthesized N,S-codoped TiO_2/MMT

CCD MODEL AND ANOVA ANALYSIS

Response surface methodology (RSM) was applied to analyze and optimize Cip photocatalytic degradation by N,S-codoped TiO_2/MMT. For this purpose, 30 experiments were carried out for response surface modeling. The design of the experiment according to CCD and the experimental results for photocatalytic degradation runs are presented in Table 3.

The quadratic equation for Cip degradation efficiency is expressed according to Eq. (2) and (3) for coded and actual factors respectively:

$$\text{Removal}\ (\%) = 86.25 - 5.13\times A + 3.58 \times B - 4.42 \times C + 3.62 \times D + 1.75 \times AB - 3.00 \times AC + 0.69 \times BD - 2.72 \times A^2 - 2.03 \times B^2 - 1.53 \times C^2 - 1.16 \times D^2 \quad (2)$$

$$\text{Removal}\ (\%) = + 17.19677 + 3.28750 \times \text{Cip} + 0.69867 \times \text{Catalyst} + 7.65104 \times \text{pH} + 0.30300 \times \text{Reaction time}$$

Table 3. Design of experiments according to CCD along and the results of observed responses

Run	Antibiotic [mg L^{-1}]	Catalyst [mg L^{-1}]	pH	Reaction time [mine]	Degradation [%]	
					Experimental	Predicted
1	20	50	9	90	77	75.9
2	20	25	9	40	57.5	58.0
3	20	25	5	90	79	78.7
4	10	50	5	90	92	91.5
5	20	50	9	40	66	67.3
6	15	38	7	65	86.5	86.3
7	5	38	7	65	84.5	85.6
8	10	25	9	40	79	77.8
9	20	50	5	90	89.5	90.8
10	15	38	7	65	86.5	86.3
11	10	50	9	40	81	80.0
12	20	50	5	40	81	82.1
13	15	13	7	65	71	71.0
14	15	38	7	65	87	86.3
15	15	63	7	65	86	85.3
16	10	25	5	40	81	80.6
17	10	50	5	40	82	82.9
18	15	38	7	65	86	86.3
19	10	25	5	90	86.5	86.5
20	25	38	7	65	67	65.1
21	15	38	3	65	90	89.0
22	15	38	11	65	71	71.3
23	20	25	5	40	72	72.8
24	15	38	7	65	87	86.3
25	10	50	9	90	86.5	88.7
26	15	38	7	65	84.5	86.3
27	15	38	7	115	90	88.9
28	20	25	9	90	63	63.9
29	15	38	7	15	74	74.4
30	10	25	9	90	83	83.6

$+ 0.02800 \times Cip \times Catalyst - 0.30000 \times Cip \times pH + 0.00220 \times Catalyst \times Reaction\ time - 0.10875 \times Cip^2 - 0.013000 \times Catalyst^2 - 0.38281 \times pH^2 - 0.00185 \times Reaction\ time^2$ (3)

The degree of accuracy and significance of the suggested regression model was evaluated using R^2, adjusted R^2 (adjusted determination coefficient), F-value, and P-value[33]. By comparing the experimental results and the predicted responses calculated by the model, according to Equation 3, it was found that the predicted values were proportional to the values of the experimental results[33]. Also, the fitting of the estimated model with data can be evaluated by value of R^2, which varies from 0 to 1. R^2 value of 0.9840 for degradation proposed that the obtained regression equations can be applied to predict the degradation percent of Cip in the experiment range[33]. The high values of R^2 (0.9840) and Adj-R^2 (0.9742) represent a high correlation between the results of the experiment and the predicted responses[34]. As shown in Table 4 the F-value for the model is 100. This value indicates that the quadratic polynomial response equation was significant. There is only a 0.01% chance that a "Model F-Value" could occur by reason of noise. The P-value of the model, which is < 0.0001, demonstrates that the model is highly significant. Also, the insignificant lack of fit (0.13) indicates good predictability of the suggested model. The significance of each coefficient can be checked by their P-values[34]. In this study, the coefficients A, B, C, D, AB, AC, A^2, B^2 C^2, and D^2 are significant model coefficients. On the whole, the results of the Analysis of variance (ANOVA) analysis show that the model is significant for Cip removal from polluted aqueous solution.

EFFECT OF VARIABLES AS SURFACE RESPONSE PLOT

In order to determine the effect of variables, the surface response plot was used. Surface response plots provide a method to predict degradation efficiency for different values of test variables[35]. Figure 7a shows the surface response plot of photocatalytic degradation efficiency as a function of catalyst dose and initial Cip concentration at a pH of 7 and reaction time of 65 min. By decreasing the initial concentration of Cip and increasing the catalyst dose, the highest degradation of Cip is observed. The initial concentration of Cip has a greater effect on photocatalytic degradation than the catalyst dose. It is reported that as the initial concentration of the Cip increases, the degradation efficiency is reduced. The possible reason suggested for this decrease was that as the initial concentration of the Cip increased, available active sites on the nanocomposite surface are saturated. Therefore, the nanocomposite does not have the capacity to react with all the Cip molecules. This result is similar to the results of some studies on antibiotic degradation[4, 36] characterization and application of NH4Cl-induced activated carbon (NAC. On the other hand, by decreasing the initial concentration of Cip, the reaction between Cip and oxidative species is likely to increase, which leads to an improvement in degradation efficiency[4].

In this study, due to the importance of pH in the photocatalytic decomposition process, the effect of pH on Cip degradation was investigated. Figure 7b shows the surface response surface plot of photocatalytic degradation efficiency as a function of pH and initial Cip concentration in a catalyst dose of 37.5 mg L^{-1} and reaction time of 65 min. As illustrated in Figure 7b, the suitable range for pH is (5–7). The pH at which the surface of a photocatalyst is un-charged is considered as the zero point charge (pH_{zpc}). The Cip has two pK_a values (5.9 and 8.9) and can exist in cationic form ($Cip^{0,+}$) at pH lower than 5.9, zwitterionic form ($Cip^{-,+}$) at pH in range of 5.9 to 8.9, and anionic form ($Cip^{-,0}$) at pH higher than 8.9[37, 38]. Based on the zero-point charge analysis, the pH_{zpc} of the surface of N,S-codoped TiO_2/MMT nanocomposite was 6.1. This implies that the nanocomposite has a positive charge at a pH below 6.1 and a negative charge at a pH above 6.1[39]. Therefore, both nanocomposite and Cip have negative charge in high pH, leading to a repulsive force between them. On the other hand, both nanocomposite and Cip have a positive charge in low pH, leading to repulsion between them. Therefore, the photodegradation efficiency, both at low pH and at high pH, is decreased. But, it should also be noted that potential of hydroxide radicals for the oxidation of Cip increases with decreasing pH[3, 40]. Also, at pH higher than 9, due to an increase in the concentration of OH ions and their competition with negatively charged molecule (Cip), the removal efficiency can be reduced[41]. Therefore, high adsorption and high potential of hydroxyl radicals, determine the optimum pH for removal of the Cip. According to the obtained

Table 4. Analysis of variance for fit of photocatalytic degradation model

Source	Sum of Squares	df	Mean Square	F Value	p-value Prob. > F	
Model	2232.01	11	202.91	100.64	< 0.0001	Sig.
A-Cip	630.38	1	630.38	312.65	< 0.0001	
B-Catalyst	308.17	1	308.17	152.85	< 0.0001	
C-pH	468.17	1	468.17	232.20	< 0.0001	
D- time	315.37	1	315.37	156.42	< 0.0001	
AB	49.00	1	49.00	24.30	< 0.0001	
AC	144.00	1	144.00	71.42	0.0001	
BD	7.56	1	7.56	3.75	< 0.0001	
A^2	202.74	1	202.74	100.56	0.0686	
B^2	113.17	1	113.17	56.13	< 0.0001	
C^2	64.31	1	64.31	31.90	< 0.0001	
D^2	36.67	1	36.67	18.19	< 0.0001	
Residual	36.29	18	2.02			
Lack of Fit	31.92	13	2.46	2.81	0.1309	not sig.
Pure Error	4.37	5	0.87			
Cor Total	2268.37	29				

R^2 = 0.9840, Adj R^2 = 0.9742, Pred R^2 = 0.9482, Adeq precision = 37.303, Std. Dev. =1.42, C.V. % = 1.77.

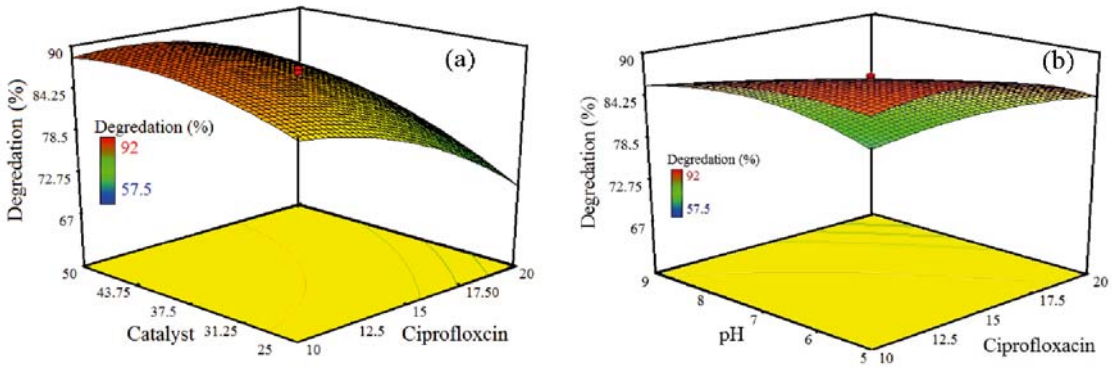

Figure 7. The surface plot of the Cip degradation efficiency as (a) the function catalyst dose/Cip concentration (b) pH/Cip concentration

model, the optimum pH for Cip degradation is 5.75. The results of this study are consistent with the results of previous studies[4, 42].

Figure 8 shows the response surface plot of photocatalytic degradation efficiency as a function of reaction time and catalyst concentration in initial Cip concentration of 15 mg L^{-1} and pH of 7. As is obvious from Figure 8, the degradation efficiency increases with increasing reaction time and catalyst concentration. An initial increase in the Cip degradation due to the increased catalyst concentration can be attributed to an increase in photon absorption on the catalyst surface and an increase in catalyst surface area. The gradual reduction of degradation rate by increasing the catalyst beyond the optimum amount is attributed to the increased turbidity of the suspension and reduction of light penetration into the solution[4, 43]. In addition, the higher loading of the catalyst can cause catalyst accumulation and decrease the total active surface, which can lead to reduced degradation[44, 45].

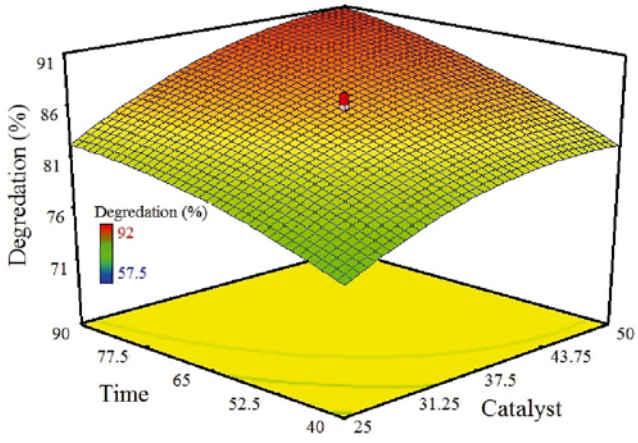

Figure 8. The surface plot of the Cip degradation efficiency as the function time/catalyst dose

DETERMINATION OF OPTIMIZED CONDITIONS

A numerical method was used to optimize Cip degradation using Design Expert 10 software. Therefore, the best target was set for each variable. To obtain optimal conditions, the experimental parameters were considered in the following ranges: the initial Cip concentration 10–20 mg L^{-1}, the catalyst dose 25–50 mg L^{-1}, the pH 5–9, and the reaction time 40–90 min. All parameters were set based on maximum desirability. The optimum values of the process variables for the maximum Cip degradation efficiency are as follow: initial Cip concentration 15 mg L^{-1}, nanocomposite concentration 46 mg L^{-1}, pH 5.75, and reaction time 90 min. The results of the experiments show that, in optimum conditions, the removal efficiency of Cip is 92% and 70% for N,S-codoped TiO_2/MMT nanocomposite and TiO_2 respectively (Fig. 9). The high removal of Cip by nanocomposite compared to TiO_2 in the photocatalytic process shows that there is a synergistic effect between nanocomposite and simulated sunlight that increases the effectiveness of the nanocomposite. The enhanced photocatalytic activity of nanocatalyst is due to non-metals doping and high crystallinity and the mesoporosity of the N,S-codoped TiO_2/MMT nanocomposite. This result is similar to those of some studies[39, 46].

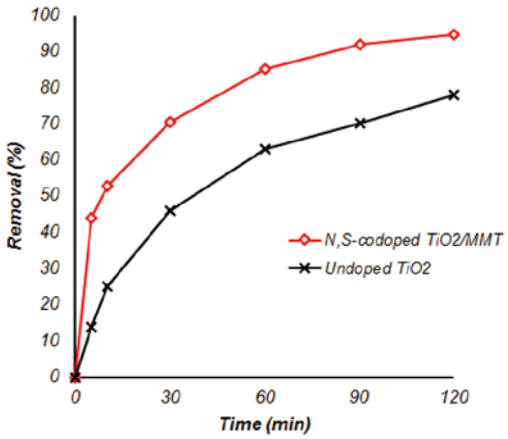

Figure 9. Comparison of photocatalytic degradation of Cip by N,S-codoped TiO_2/MMT, and TiO_2

REUSABILITY OF NANOCOMPOSITE

Reusability experiments were conducted under optimum conditions. After each run, the obtained solution was centrifuged and the photocatalyst was rinsed with water. The process was repeated four times. The results show that the degradation level of the photocatalyst decreased from 92% in the first run to 66% after four runs (Fig. 10).

MINERALIZATION STUDIES

In order to determine the mineralization, the total organic carbon of the samples was tested under optimum conditions. The results showed that with the application of synthesized nanocomposite under optimal conditions, 32% mineralization can be achieved.

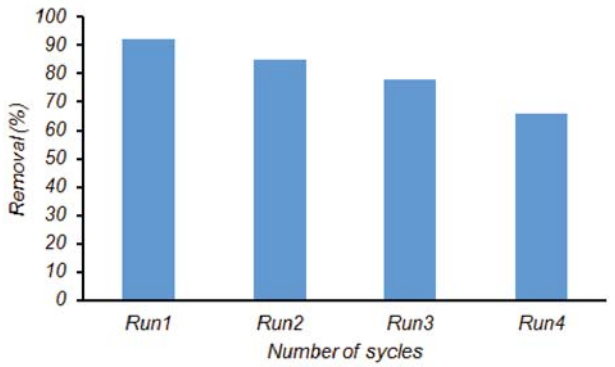

Figure 10. Application of nanocomposite in consecutive runs for removal of Cip

CONCLUSIONS

The N,S-codoped TiO_2/MMT nanocomposite material, which consists of MMT, TiO_2, and dopants (N and S), has been synthesized through the sol-gel method. The results of XRD and FESEM of nanocomposites show that the N,S-codoped TiO_2 nanoparticles were been immobilized on the surface of MMT. The band gap of synthesized nanocomposite decreased from 3.17 to 2.77 eV. Reducing the nanocomposite band gap increases its photocatalytic activity by exposing visible light. At optimized conditions (pH = 5.75, catalyst dose = 46 mg L^{-1}, initial Cip concentration = 15 mg L^{-1} and reaction time = 90 min), the maximum degradation and mineralization efficiency of Cip was 92% and 32% respectively. The reusability of nanocomposite results shows that with the use of nanocomposite in the four consecutive runs, the final removal efficiency was 66%. The results show that the N,S-codoped TiO_2/MMT nanocomposite under simulated sunlight irradiation can be used as an effective method for the removal of Cip from aqueous solutions.

ACKNOWLEDGMENTS

The authors thank Shahid Beheshti University of Medical Sciences, Tehran, Iran (grant 9095.11) for their financial support to this research project.

LITERATURE CITED

1. Klavarioti, M., Mantzavinos, D. & Kassinos, D. (2009). Removal of residual pharmaceuticals from aqueous systems by advanced oxidation processes. *Environ. Int.* 35(2)**,** 402–417. DOI: 10.1016/j.envint.2008.07.009.

2. Parsa, J.B., Panah, T.M. & Chianeh, F.N. (2016). Removal of ciprofloxacin from aqueous solution by a continuous flow electro-coagulation process. *Korean J. Chem. Eng.* 33(3), 893–901. DOI: 10.1007/s11814-015-0196-6.

3. Hassani, A., Khataee, A., Karaca, S., Karaca, C. & Gholami, P. (2016). Sonocatalytic degradation of ciprofloxacin using synthesized TiO_2 nanoparticles on montmorillonite. *Ultrason. Sonochem.* 35, 1–12. DOI: 10.1016/j.ultsonch.2016.09.027.

4. Hassani, A., Khataee, A. & Karaca, S. (2015). Photocatalytic degradation of ciprofloxacin by synthesized TiO_2 nanoparticles on montmorillonite: Effect of operation parameters and artificial neural network modeling. *J. Mol. Catal. A Chem.* 409, 149–161. DOI: 10.1016/j.molcata.2015.08.020.

5. Gharbani, P., Mehrizad, A. & Jafarpour, I. (2015). Adsorption of penicillin by decaffeinated tea waste. *Polish J. Chem. Technol.* 17(3), 95–9. DOI: 10.1515/pjct-2015-0056.

6. Hassani, A., Khataee, A., Karaca, S. & Fathinia, M. (2017). Degradation of mixture of three pharmaceuticals by photocatalytic ozonation in the presence of TiO2/montmorillonite nanocomposite: Simultaneous determination and intermediates identification. *J. Environ. Chem. Eng.* 5(2), 1964–76. DOI: 10.1016/j.jece.2017.03.032.

7. Hassani, A., Khataee, A., Fathinia, M. & Karaca, S. (2018). Photocatalytic ozonation of ciprofloxacin from aqueous solution using TiO2/MMT nanocomposite: Nonlinear modeling and optimization of the process via artificial neural network integrated genetic algorithm. *Process Saf. Environ. Prot.* 116, 365–76. DOI: 10.1016/j.psep.2018.03.013.

8. Kümmerer, K. (2009). Antibiotics in the aquatic environment – A review – Part I. *Chemosphere* 75(4), 417–434. DOI: 10.1016/j.chemosphere.2008.11.086.

9. Ghasemi, Z., Younesi, H. & Zinatizadeh, A.A. (2016). Preparation, characterization and photocatalytic application of TiO_2/ Fe-ZSM-5 nanocomposite for the treatment of petroleum refinery wastewater: Optimization of process parameters by response surface methodology. *Chemosphere* 159, 552–564. DOI: 10.1016/j.chemosphere.2016.06.058.

10. Daghrir, R., Drogui, P., Delegan, N. & Khakani, M.A.E. (2013). Electrochemical degradation of chlortetracycline using N-doped Ti/TiO2 photoanode under sunlight irradiations. *Water Res.* 47(17), 6801–10. DOI: 10.1016/j.watres.2013.09.011.

11. Wojcieszak, D., Mazur, M., Kaczmarek, D., Morgiel, J., Poniedziałek, A. & Domaradzki, J., et al. (2015). Influence of the structural and surface properties on photocatalytic activity of TiO_2:Nd thin films. *Polish J. Chem. Technol.* 17(2), 103–11. DOI: 10.1515/pjct-2015-0047.

12. Dulian, P., Buras, M. & Witold, Ż. (2016). Modyfication of photocatalytic properties of titanium dioxide by mechanochemical method. *Polish J. Chem. Technol.* (110), 68–71.

13. Rengifo-Herrera, J.A., Pierzchala, K., Sienkiewicz, A., Forro, L., Kiwi, J., Moser, J.E. & Pulgarin, C. (2010). Synthesis, characterization, and photocatalytic activities of nanoparticulate N, S-codoped TiO2 having different surface-to-volume ratios. *J. Phys. Chem. C.* 114(6), 2717–2723. DOI: 10.1021/jp910486f.

14. Li, Y. & Kim, S.J. (2005). Synthesis and characterization of nano titania particles embedded in mesoporous silica with both high photocatalytic activity and adsorption capability. *J. Phys. Chem. B.,* 109(25)**,** 12309–12315. DOI: 10.1021/jp0512917.

15. Zhang, G., Ding, X., Hu, Y., Huang, B., Zhang, X. & Qin, X., et al. (2008). Photocatalytic Degradation of 4BS Dye by N, S-Codoped TiO_2 Pillared Montmorillonite Photocatalysts under Visible-Light Irradiation. *J. Phys. Chem. C.,* 112, 17994–17997. DOI: 10.1016/j.jpcs.2007.10.090.

16. Eslami, A., Amini, MM., Yazdanbakhsh, AR., Mohseni-Bandpei, A., Safari, AA. & Asadi, A. (2016). N,S co-doped TiO2 nanoparticles, and nanosheets in simulated solar light for photocatalytic degradation of non-steroidal anti-inflammatory drugs in water: a comparative study. *J. Chem. Technol. Biotechnol.* 91(10), 2693–2704. DOI: 10.1002/jctb.4877.

17. Xiang, Q., Yu, J. & Jaroniec, M. (2011). Nitrogen and sulfur co-doped TiO2 nanosheets with exposed {001} facets: synthesis, characterization and visible-light photocatalytic activity. *Phys. Chem. Chem. Phys.* 13(11), 4853–61. DOI: 10.1039/C0CP01459A.

18. Wu, Q., Li, Z., Hong, H., Yin, K. & Tie, L. (2010). Adsorption and intercalation of ciprofloxacin on montmorillonite. *Appl. Clay Sci.* 50(2), 204–211. DOI:10.1016/j.clay.2010.08.001

19. Yuan, L., Huang, D., Guo, W., Yang, Q. & Yu, J. (2011). TiO_2/montmorillonite nanocomposite for removal of organic pollutant. *Appl. Clay. Sci.* 53(2), 272–278. DOI: 10.1016/j.clay.2011.03.013.

20. Carrasquillo, A.J., Bruland, G.L., Mackay, A.A. & Vasudevan, D. (2008). Sorption of ciprofloxacin and oxytetracycline zwitterions to soils and soil minerals: Influence of compound structure. *Environ. Sci. Technol.* 42(20), 7634–7642. DOI: 10.1021/es801277y.

21. Sun, H., Peng, T., Liu, B. & Xian, H. (2015). Effects of montmorillonite on phase transition and size of TiO2 nanoparticles in TiO2/montmorillonite nanocomposites. *Appl. Clay Sci.* 114, 440–446. DOI: 10.1016/j.clay.2015.06.026.

22. Kameshima, Y., Tamura, Y. Nakajima, A. & Okada, K. (2009). Preparation and properties of TiO2/montmorillonite composites. *Appl. Clay Sci.* 45(1–2), 20–3. DOI: 10.1016/j.clay.2009.03.005.

23. An, T., Chen, J., Li, G., Ding, X., Sheng, G. & Fu, J., et al. (2008). Characterization and the photocatalytic activity of TiO_2 immobilized hydrophobic montmorillonite photocatalysts. Degradation of decabromodiphenyl ether (BDE 209). *Catal. Today* 139(1–2), 69–76. DOI: 10.1016/j.cattod.2008.08.024.

24. Chen, D., Du, G., Zhu, Q. & Zhu, F. (2013). Synthesis and characterization of TiO_2 pillared montmorillonites: Application for methylene blue degradation. *J. Colloid Interface Sci.* 409, 151–7. DOI: 10.1016/j.jcis.2013.07.049.

25. Shaban, Y.A. & Khan, S.U.M. (2009). Carbon modified (CM)-n-TiO2 thin films for efficient water splitting to H_2 and O_2 under xenon lamp light and natural sunlight illuminations. *J. Solid State Electrochem.* 13(7), 1025–36. DOI: 10.1007/s10008-009-0823-4.

26. Zhang, G., Ding, X, He, F., Yu, X., Zhou, J. & Hu, Y., et al. (2008). Preparation and photocatalytic properties of TiO2--montmorillonite doped with nitrogen and sulfur. *J. Phys. Chem. Solids.* 69(5-6), 1102–1106. DOI: 10.1016/j.jpcs.2007.10.090.

27. Sohrabi, S. & Akhlaghian, F. (2016). Modeling and optimization of phenol degradation over copper-doped titanium dioxide photocatalyst using response surface methodology. *Process Saf. Environ. Prot.* 99, 120–128. DOI: 10.1016/j.psep.2015.10.016.

28. Karimi, L. (2017). Combination of mesoporous titanium dioxide with MoS2 nanosheets for high photocatalytic activity. *Polish J. Chem. Technol.* 19(2), 56–60. DOI: 10.1515/pjct-2017-0028.

29. Fatimah, I., Wang, S. & Wulandari, D. (2011). ZnO/montmorillonite for photocatalytic and photochemical degradation of methylene blue. *Appl. Clay Sci.* 53(4), 553–560. DOI: 10.1016/j.clay.2011.05.001.

30. Kattiparambil Manoharan, R. & Sankaran, S. (2017). Photocatalytic degradation of organic pollutant aldicarb by non-metal-doped nanotitania: synthesis and characterization. *Environ. Sci. Pollut. Res.* DOI: 10.1007/s11356-017-0350-2.

31. Liu, J., Li, X., Zuo, S. & Yu, Y. (2007). Preparation and photocatalytic activity of silver and TiO2 nanoparticles/montmorillonite composites. *Appl. Clay Sci.* 37(3), 275–280. DOI: 10.1016/j.clay.2007.01.008.

32. Han, C., Pelaez, M., Likodimos, V., Kontos, AG, Falaras, P. & O'Shea, K., et al. (2011). Innovative visible light-activated sulfur doped TiO_2 films for water treatment. *Appl. Catal. B. Environ.* 107(1–2), 77–87. DOI: 10.1016/j.apcatb.2011.06.039.

33. Salarian, A.A., Hami, Z., Mirzaie, N., Mohseni, SM., Asadi, A. & Bahrami, H, et al. (2016). N-doped TiO_2 nanosheets for photocatalytic degradation and mineralization of diazinon under simulated solar irradiation: Optimization and modeling using a response surface methodology. *J. Mol. Liq.* 220, 183–191. DOI: 10.1016/j.molliq.2016.04.060.

34. Rasouli, F., Aber, S., Salari, D. & Khataee, A.R. (2014). Optimized removal of Reactive Navy Blue SP-BR by organo-montmorillonite based adsorbents through central composite design. *Appl. Clay Sci.* 87, 228–234. DOI: 10.1016/j.clay.2013.11.010.

35. Khataee, A.R., Zarei, M. & Asl, S.K. (2010). Photocatalytic treatment of a dye solution using immobilized TiO2 nanoparticles combined with photoelectro-Fenton process: Optimization of operational parameters. *J. Electroanal. Chem.* 648, 143–150. DOI: 10.1016/j.jelechem.2010.07.017.

36. Moussavi, G., Alahabadi, A., Yaghmaeian, K. & Eskandari, M. (2013). Preparation, characterization and adsorption potential of the NH4Cl-induced activated carbon for the removal of amoxicillin antibiotic from water. *Chem. Eng. J.* 217, 119–28. DOI: 10.1016/j.cej.2012.11.069.

37. Carmosini, N. & Lee, L.S. (2009). Ciprofloxacin sorption by dissolved organic carbon from reference and bio-waste materials. *Chemosphere* 77, 813–820. DOI: 10.1016/j.chemosphere.2009.08.003.

38. Gu, C. & Karthikeyan, K.G. (2005). Sorption of the antimicrobial ciprofloxacin to aluminum and iron hydrous oxides. *Environ. Sci. Technol.* 39(23), 9166–9173. DOI: 10.1021/es051109f.

39. Abdullah, A.H., Moey, H.J.M. & Yusof, N.A. (2012). Response surface methodology analysis of the photocatalytic removal of Methylene Blue using bismuth vanadate prepared via polyol route. *J. Environ. Sci. (China)* 24(9), 1694–701. DOI: 10.1016/S1001-0742(11)60966-2.

40. An, T., Yang, H., Li, G., Song, W., Cooper W.J. & Nie, X. (2010). Kinetics and mechanism of advanced oxidation processes (AOPs) in degradation of ciprofloxacin in water. *Appl. Catal. B Environ.* 94(3–4), 288–94. DOI: 10.1016/j.apcatb.2009.12.002.

41. Massoudinejad, M., Ghaderpoori, M., Shahsavani, A., Jafari, A., Kamarehie, B., Ghaderpoury, A. & Amini, M.M. (2018). Ethylenediamine-functionalized cubic ZIF-8 for arsenic adsorption from aqueous solution: Modeling, isotherms, kinetics and thermodynamics. *J. Mol. Liq.* 255, 263–8. DOI: 10.1016/j.molliq.2018.01.163.

42. Gad-Allah, T.A., Ali, M.E.M.M. & Badawy, M.I. (2011). Photocatalytic oxidation of ciprofloxacin under simulated sunlight. *J. Hazard. Mater.* 186(1), 751–755. DOI: 10.1016/j.jhazmat.2010.11.066.

43. Kuriechen, S.K., Murugesan, S., Raj, S.P. & Maruthamuthu, P. (2011). Visible light assisted photocatalytic mineralization of Reactive Red 180 using colloidal TiO_2 and oxone. *Chem. Eng. J.* 174(2–3), 530–538. DOI: 10.1016/j.cej.2011.09.024.

44. Modirshahla, N., Hassani, A., Behnajady, M.A. & Rahbarfam, R. (2011). Effect of operational parameters on decolorization of Acid Yellow 23 from wastewater by UV irradiation using ZnO and ZnO/SnO_2 photocatalysts. *Desalination* 271(1–3), 187–192. DOI: 10.1016/j.desal.2010.12.027.

45. Akbari-Adergani, B., Saghi, M.H., Eslami, A., Mohseni--Bandpei, A. & Rabbani, M. (2017). Removal of Dibutyl Phthalate from Aqueous Environments Using a Nanophotocatalytic Fe, Ag-ZnO/VIS-LED System: Modeling and Optimization. *Environ. Technol.* 0, 1–31. DOI: 10.1080/09593330.2017.1332693.

46. El-Sheikh, S.M., Zhang, G., El-Hosainy, H.M., Ismail, A.A., O'Shea, K.E., Falaras, P., Kontos, A.G. & Dionysiou, D.D. (2014). High performance sulfur, nitrogen and carbon doped mesoporous anatase-brookite TiO_2 photocatalyst for the removal of microcystin-LR under visible light irradiation. *J. Hazard. Mater.* 280, 723–33. DOI: 10.1016/j.jhazmat.2014.08.038.